ANALYSIS OF RIGID MONOPILES IN MULTILAYERED SOIL

Bipin Kumar Gupta & Dipanjan Basu
Department of Civil & Environmental Engineering, University of Waterloo, Waterloo, Ontario, Canada

GEOQuébec 2015
Challenges from North to South
Des défis du Nord au Sud

ABSTRACT
A continuum-based analysis for laterally loaded rigid monopiles supporting offshore wind turbines in multilayered elastic soil is presented. The principle of virtual work is used to derive the equilibrium equations maintaining appropriate force balance between the pile and soil. The equilibrium equations are solved using an iterative numerical scheme to obtain the pile and soil displacements. Pile responses obtained using this method match well with those of equivalent finite element analysis.

RÉSUMÉ
Cet article présente une analyse réalisée en milieu continu, de pieux rigides chargés latéralement dans un sol élastique multicouches qui supportent des éoliennes situées en mer. Le principe du travail virtuel est utilisé pour dériver les équations d'équilibre qui permettent le maintien de l'équilibre de la force exercée entre le pieu et le sol. Les équations d'équilibre sont résolues avec un système numérique itératif et permettent le calcul des déplacements du pieu et du sol. Les résultats obtenus grâce à cette méthode correspondent bien à ceux obtenus avec une analyse par éléments finis.

1 INTRODUCTION

Monopiles for offshore wind turbines are large diameter (4-6 m) cylindrical piles installed into the sea bed to a depth of about 5-6 times the diameter (Klinkvort and Hededal 2014). These piles are mostly subjected to lateral forces and moments at the head arising from wind, wave, and water currents. Several researchers performed centrifuge tests and finite element (FE) analysis of monopiles in sandy and clayey soils to investigate their load-displacement behavior (Klinkvort and Hededal 2012, Haiderali et al. 2013), and reported that monopiles undergo deformations typically by rigid-body rotation about a pivot point.

For monopiles supporting an offshore wind turbine, the allowable lateral head displacement and rotation is an important design criterion. The methods available for analysis of laterally loaded rigid piles are mostly based on the theories of ultimate capacity (Broms 1964a, b, Meyerhoff and Ranjan 1972, Zhang et al. 2005) that cannot be used to obtain the load-displacement response under serviceability conditions. In the literature, very few studies exist that focus on the load-displacement response of rigid piles under serviceability conditions (Higgins et al. 2013, Motta 2013).

In this study, a new method for analysis of laterally-loaded rigid monopiles in multilayered, elastic soil is presented in which rational soil and pile displacement fields ensuring compatibility and continuity are assumed to obtain the equilibrium equations using the principle of virtual work. The equilibrium equations are solved analytically and numerically to calculate the pile head displacement and rotation. Pile responses obtained from this analysis are found to be in good agreement with those obtained from equivalent three-dimensional (3D) FE analysis. The advantage of the analysis is that it produces results fast and without any cumbersome input of pile geometry and mesh, as required in 3D FE analysis.

2 ANALYSIS

The analysis is based on the principles of continuum mechanics in which the soil is treated as a 3D elastic continuum.

2.1 Problem definition

Figure 1 shows a rigid monopile in a multilayered elastic soil deposit with each layer i characterized by Lame's constants λ_{si} and G_{si} and thickness $H_i - H_{i-1}$ ($H_0 = 0$).

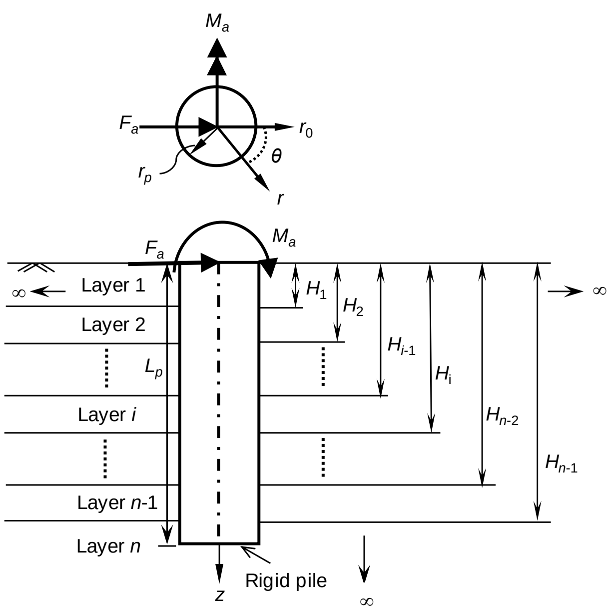

Figure 1. A laterally loaded rigid monopile in multilayered elastic soil deposit

Each layer has infinite radial extent and the bottom (n^{th}) layer has infinite extent in downward vertical direction as well. The pile head is at the ground surface and subjected to a horizontal force F_a and a moment M_a, and the base is embedded in the n^{th} layer. No slippage or separation between the pile and the surrounding soil or between the soil layers is allowed. The goal of the analysis is to obtain head displacement and rotation caused by the action of F_a and/or M_a for which a cylindrical (r-θ-z) coordinate system is assumed.

2.2 Force diagram of pile-soil system

Figure 2 shows the force diagrams of the pile and soil separately. The interaction between soil and pile is captured by the distributed soil reaction force p acting along the pile shaft and by the concentrated shear force S_b at the pile base. The distributed reaction p is the resistance offered by the soil layers surrounding the pile against the lateral movement and rotation of pile, and the base shear force S_b is the resistance offered by the soil layers beneath the pile against its lateral movement. These force diagrams are used to obtain the equilibrium equations.

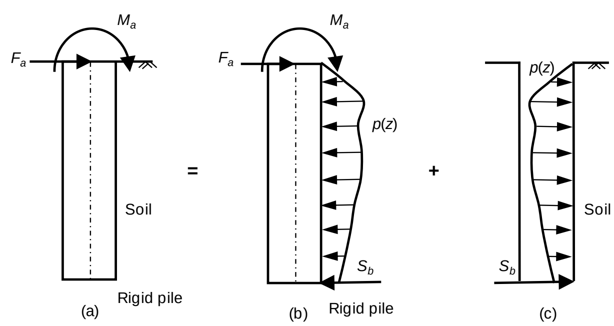

Figure 2. (a) A rigid pile-soil system, (b) forces acting on pile, and (c) forces acting on soil

2.3 Displacement profile of the rigid pile

For a pile undergoing displacement typically by rigid body rotation and translation, it is reasonable to assume a linear displacement profile (Figure 3) as

$$w(z) = w_h - \Theta_h z \qquad [1]$$

where w is the lateral pile displacement varying with depth z, w_h is the pile head displacement, and Θ_h is the clockwise rotation of pile axis in the vertical plane in which F_a acts.

2.4 Application of principle of virtual work to rigid pile

The principle of virtual work states that $\delta W_E - \delta W_I = 0$ where δW_E is the external virtual work and δW_I is the internal virtual work. Applying the principle of virtual work to the rigid pile (Figure 2b), and using Eq. [1] results in

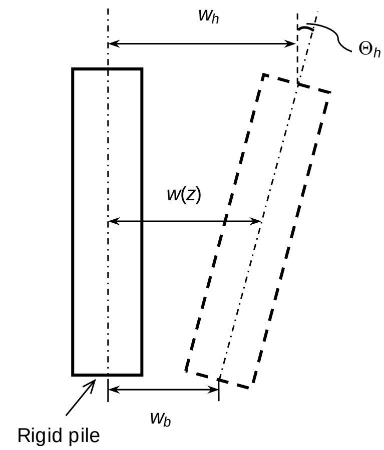

Figure 3. Assumed rigid pile displacement profile

$$\left[F_a - \int_0^{L_p} p(z)dz - S_b\right]\delta w_h + \left[M_a + \int_0^{L_p} p(z)zdz + S_b L_p\right]\delta\Theta_h = 0 \qquad [2]$$

Since $\delta w_h \neq 0$ and $\delta\Theta_h \neq 0$ as w_h and Θ_h are arbitrary,

$$F_a = \int_0^{L_p} p(z)dz + S_b \qquad [3]$$

$$M_a = -\left[\int_0^{L_p} p(z)zdz + S_b L_p\right] \qquad [4]$$

2.5 Displacements, strains and stress profile for soil

The displacements in soil are assumed as

$$u_r = w(z)\phi_r(r)cos\theta \qquad [5]$$

$$u_\theta = -w(z)\phi_\theta(r)sin\theta \qquad [6]$$

$$u_z = 0 \qquad [7]$$

where ϕ_r and ϕ_θ are dimensionless displacement functions varying with radial coordinate r, and θ is the angle measured clockwise from a vertical reference section ($r = r_0$) that contains the applied loading. The functions $\phi_r(r)$ and $\phi_\theta(r)$ ensures perfect contact between pile and soil and that the displacements within the soil mass (due to pile displacement) decrease monotonically with increase in radial distance from the pile axis. Therefore, ϕ_r and ϕ_θ varies between 1 at the pile-soil interface and 0 at infinite radial distance from the pile.

Differentiation of the displacement fields in Eqs. [5]-[7] leads to the following strain-displacement relationships for the soil mass (contractive strains are assumed positive)

$$\begin{bmatrix} \varepsilon_{rr} \\ \varepsilon_{\theta\theta} \\ \varepsilon_{zz} \\ \gamma_{r\theta} \\ \gamma_{rz} \\ \gamma_{\theta z} \end{bmatrix} = \begin{bmatrix} -w(z)\dfrac{d\phi_r(r)}{dr}\cos\theta \\ -w(z)\dfrac{\phi_r(r)-\phi_\theta(r)}{r}\cos\theta \\ 0 \\ w(z)\left\{\dfrac{\phi_r(r)-\phi_\theta(r)}{r}+\dfrac{d\phi_\theta(r)}{dr}\right\}\sin\theta \\ -\dfrac{dw(z)}{dz}\phi_r(r)\cos\theta \\ \dfrac{dw(z)}{dz}\phi_\theta(r)\sin\theta \end{bmatrix} \quad [8]$$

The elastic stress-strain relationship is given by

$$\sigma_{lm} = \lambda_s\delta_{lm}\varepsilon_{nn} + 2G_s\varepsilon_{lm} \quad [9]$$

where λ_s and G_s are Lame's constants for a soil layer, σ_{lm} and ε_{lm} are the stress and strain tensors, respectively, and δ_{lm} is the Kronecker's delta expressed in indicial notations.

2.6 Application of principle of virtual work to soil

Application of the principle of virtual work to the soil mass (Figure 2c) results in

$$\int_0^{L_p} p(z)\,\delta w\,dz + S_b\delta w_b - \int_0^{\infty}\int_0^{2\pi}\int_{r_p}^{\infty}\sigma_{lm}\delta\varepsilon_{lm}\,r\,dr\,d\theta\,dz - \int_{L_p}^{\infty}\int_0^{2\pi}\int_{r_p}^{\infty}\sigma_{lm}\delta\varepsilon_{lm}\,r\,dr\,d\theta\,dz = 0 \quad [10]$$

where $\delta\varepsilon_{lm}$ is the virtual strain in the soil mass due to the virtual displacement applied on the rigid pile.

Substituting Eqs. [8] and [9] in Eq. [10] to calculate $\sigma_{lm}\delta\varepsilon_{lm}$ modifies Eq. [10] as

$$\left[A(w)\delta w + B(w)\delta\left(\frac{dw}{dz}\right)\right] + \left[C(\phi_r)\delta\phi_r\right] + \left[D(\phi_\theta)\delta\phi_\theta\right] = 0 \quad [11]$$

where δw, $\delta\phi_r$ and $\delta\phi_\theta$ are the first variation of the functions $w(z)$, $\phi_r(r)$ and $\phi_\theta(r)$.

2.7 Soil displacement profile

Equating the terms associated with $\delta\phi_r$ in Eq. [11] to zero because of its non-zero variation in the interval $r_p \le r \le \infty$, the following differential equation is obtained:

$$\frac{d^2\phi_r}{dr^2} + \frac{1}{r}\frac{d\phi_r}{dr} - \left[\left(\frac{\gamma_1}{r}\right)^2 + \left(\frac{\gamma_2}{r_p}\right)^2\right]\phi_r = \frac{\gamma_3^2}{r}\frac{d\phi_\theta}{dr} - \left(\frac{\gamma_1}{r}\right)^2\phi_\theta \quad [12]$$

along with the boundary conditions $\phi_r = 1$ at $r = r_p$ and $\phi_r = 0$ at $r = \infty$. The dimensionless constants γ_1, γ_2 and γ_3 in Eq. [12] are given by

$$\gamma_1 = \sqrt{\frac{\sum_{i=1}^{n}(\lambda_{si}+3G_{si})\int_{H_{i-1}}^{H_i}(w_h-\Theta_h z)^2 dz + (\lambda_{sn}+3G_{sn})(w_h-\Theta_h L_p)^2\sqrt{\dfrac{\zeta t_n}{2k_n}}}{\sum_{i=1}^{n}(\lambda_{si}+2G_{si})\int_{H_{i-1}}^{H_i}(w_h-\Theta_h z)^2 dz + (\lambda_{sn}+2G_{sn})(w_h-\Theta_h L_p)^2\sqrt{\dfrac{\zeta t_n}{2k_n}}}} \quad [13]$$

$$\gamma_2 = r_p\sqrt{\frac{\sum_{i=1}^{n}G_{si}\int_{H_{i-1}}^{H_i}\Theta_h^2 dz + G_{sn}(w_h-\Theta_h L_p)^2\sqrt{\dfrac{k_n}{8\zeta t_n}}}{\sum_{i=1}^{n}(\lambda_{si}+2G_{si})\int_{H_{i-1}}^{H_i}(w_h-\Theta_h z)^2 dz + (\lambda_{sn}+2G_{sn})(w_h-\Theta_h L_p)^2\sqrt{\dfrac{\zeta t_n}{2k_n}}}} \quad [14]$$

$$\gamma_3 = \sqrt{\frac{\sum_{i=1}^{n}(\lambda_{si}+G_{si})\int_{H_{i-1}}^{H_i}(w_h-\Theta_h z)^2 dz + (\lambda_{sn}+G_{sn})(w_h-\Theta_h L_p)^2\sqrt{\dfrac{\zeta t_n}{2k_n}}}{\sum_{i=1}^{n}(\lambda_{si}+2G_{si})\int_{H_{i-1}}^{H_i}(w_h-\Theta_h z)^2 dz + (\lambda_{sn}+2G_{sn})(w_h-\Theta_h L_p)^2\sqrt{\dfrac{\zeta t_n}{2k_n}}}} \quad [15]$$

in which $\zeta = t_{n+1}/t_n$. Note that the n^{th} (bottom) layer is artificially split into two sub-layers above and below the pile base, and the sub-layer below the pile base is denoted by the subscript $n+1$ (i.e., $H_n = L_p$ and $H_{n+1} \to \infty$).

Equating the terms associated with $\delta\phi_\theta$ in Eq. [11] to zero, the following differential equation is obtained

$$\frac{d^2\phi_\theta}{dr^2}+\frac{1}{r}\frac{d\phi_\theta}{dr}-\left[\left(\frac{\gamma_4}{r}\right)^2+\left(\frac{\gamma_5}{r_p}\right)^2\right]\phi_\theta = -\frac{\gamma_6^2}{r}\frac{d\phi_r}{dr}-\left(\frac{\gamma_4}{r}\right)^2\phi_r \quad [16]$$

along with the boundary conditions $\phi_\theta = 1$ at $r = r_p$ and $\phi_\theta = 0$ at $r = \infty$. The dimensionless constants γ_4, γ_5 and γ_6 in Eq. [16] are given by

$$\gamma_4 = \sqrt{\frac{\sum_{i=1}^{n}\left(\lambda_{si}+3G_{si}\right)\int_{H_{i-1}}^{H_i}\left(w_h-\Theta_h z\right)^2 dz + \left(\lambda_{sn}+3G_{sn}\right)\left(w_h-\Theta_h L_p\right)^2\sqrt{\frac{\zeta t_n}{2k_n}}}{\sum_{i=1}^{n}G_{si}\int_{H_{i-1}}^{H_i}\left(w_h-\Theta_h z\right)^2 dz + G_{sn}\left(w_h-\Theta_h L_p\right)^2\sqrt{\frac{\zeta t_n}{2k_n}}}} \quad [17]$$

$$\gamma_5 = r_p\sqrt{\frac{\sum_{i=1}^{n}G_{si}\int_{H_{i-1}}^{H_i}\Theta_h^2 dz + G_{sn}\left(w_h-\Theta_h L_p\right)^2\sqrt{\frac{k_n}{8\zeta t_n}}}{\sum_{i=1}^{n}G_{si}\int_{H_{i-1}}^{H_i}\left(w_h-\Theta_h z\right)^2 dz + G_{sn}\left(w_h-\Theta_h L_p\right)^2\sqrt{\frac{\zeta t_n}{2k_n}}}} \quad [18]$$

$$\gamma_6 = \sqrt{\frac{\sum_{i=1}^{n}\left(\lambda_{si}+G_{si}\right)\int_{H_{i-1}}^{H_i}\left(w_h-\Theta_h z\right)^2 dz + \left(\lambda_{sn}+G_{sn}\right)\left(w_h-\Theta_h L_p\right)^2\sqrt{\frac{\zeta t_n}{2k_n}}}{\sum_{i=1}^{n}G_{si}\int_{H_{i-1}}^{H_i}\left(w_h-\Theta_h z\right)^2 dz + G_{sn}\left(w_h-\Theta_h L_p\right)^2\sqrt{\frac{\zeta t_n}{2k_n}}}} \quad [19]$$

2.8 Pile displacement profile

Equating the terms associated with δw and $\delta(dw/dz)$ to zero in Eq. [11], the following equation is obtained:

$$\sum_{i=1}^{n}\int_{H_{i-1}}^{H_i} p_i(z)\,\delta w_i dz + S_b\delta w_{n+1} - \sum_{i=1}^{n}\int_{H_{i-1}}^{H_i}\left\{k_i w_i \delta w_i - 2t_i\left(\frac{dw_i}{dz}\right)\delta\left(\frac{dw_i}{dz}\right)\right\}dz - \int_{L_p}^{\infty} 2t_{n+1}\frac{dw_{n+1}}{dz}\delta\left(\frac{dw_{n+1}}{dz}\right)dz = 0 \quad [20]$$

where

$$t_i = \begin{cases} \frac{\pi}{2}G_{si}\left[\int_{r_p}^{\infty}\left(\phi_r^2+\phi_\theta^2\right)rdr\right]; i = 1,2,\ldots,n \\ \frac{\pi}{2}G_{sn}\left[\int_{r_p}^{\infty}\left(\phi_r^2+\phi_\theta^2\right)rdr + r_p^2\right]; i = n+1 \end{cases} \quad [21]$$

$$k_i = \pi\left[\left(\lambda_{si}+2G_{si}\right)\int_{r_p}^{\infty} r\left(\frac{d\phi_r}{dr}\right)^2 dr + G_{si}\int_{r_p}^{\infty} r\left(\frac{d\phi_\theta}{dr}\right)^2 dr + 2\lambda_{si}\int_{r_p}^{\infty}\left(\phi_r-\phi_\theta\right)\frac{d\phi_r}{dr}dr + 2G_{si}\int_{r_p}^{\infty}\left(\phi_r-\phi_\theta\right)\frac{d\phi_\theta}{dr}dr + \left(\lambda_{si}+3G_{si}\right)\int_{r_p}^{\infty}\frac{1}{r}\left(\phi_r-\phi_\theta\right)^2 dr\right] \quad [22]$$

The variation of $w(z)$ in the interval $L_p \le z < \infty$ is not known a priori because of which the integrand in the integral between $z = L_p$ and $z = \infty$ in Eq. [20] must be equal to zero. This result in

$$-2t_{n+1}\frac{d^2 w_{n+1}}{dz^2} + k_n w_{n+1} = 0 \quad [23]$$

The displacement w_{n+1} in the soil at infinite vertical distance is zero. Therefore the solution of Eq. [23] satisfying this boundary condition is given by

$$w_{n+1} = w_n\big|_{z=L_p}\, e^{-\sqrt{\frac{k_n}{2t_{n+1}}}(z-L_p)} \quad [24]$$

At $z = L_p$, $\delta w_{n+1} \neq 0$. Therefore, from Eq. [20] the following boundary condition is obtained

$$2t_n\left.\frac{dw_n}{dz}\right|_{z=L_p} - 2t_{n+1}\left.\frac{dw_{n+1}}{dz}\right|_{z=L_p} - S_b = 0 \quad [25]$$

Differentiating Eq. [24], substituting it in Eq. [25], and using the linear displacement function of pile (Eq. [1]) results in

$$S_b = -2t_n\Theta_h + \sqrt{2k_n\zeta t_n}\,w_b \qquad [26]$$

where w_b is the displacement at the pile base.

The integrand for each of the integrals in Eq. [20] associated with individual layer i (i.e., for each of the intervals $H_{i-1} < z < H_i$) must equate to zero (because $\delta w_i \neq 0$), which produces the following differential equation for i^{th} layer:

$$k_i w_i - 2t_i \frac{d^2 w_i}{dz^2} - p_i(z) = 0 \qquad [27]$$

Differentiating the displacement function of pile (Eq. [1]) and substituting in Eq. [27] produces

$$p_i = k_i w_i \qquad [28]$$

Substituting, Eqs. [26] and [28] into Eqs. [3] and [4] and using Eq. [1] results in

$$F_a = \left[\int_0^{L_p} k_i\left(w_h - \Theta_h z\right)dz - 2t_n\Theta_h + \sqrt{2k_n\zeta t_n}\left(w_h - \Theta_h L_p\right)\right] \qquad [29]$$

$$M_a = \left[-\int_0^{L_p} k_i\left(w_h - \Theta_h z\right)dz - \left\{-2t_n\Theta_h + \sqrt{2k_n\zeta t_n}\left(w_h - \Theta_h L_p\right)\right\}L_p\right] \qquad [30]$$

Eqs. [29] and [30] relate the head displacement and rotation of the rigid pile with the applied force and moment.

2.9 Solution algorithm

Pile head displacement w_h and rotation Θ_h can be calculated using Eqs. [29] and [30]. However, the soil parameters k_i and t_i must be known to calculate w_h and Θ_h. The parameters k_i and t_i depend on the functions ϕ_r and ϕ_θ which, in turn, depend on w_h and Θ_h through the six dimensionless constants γ_1-γ_6. Thus, an iterative algorithm is required to obtain solutions.

Initial guesses on γ_1-γ_6 are made using which ϕ_r and ϕ_θ are determined by solving Eqs. [12] and [16] iteratively using the finite difference method. From the obtained values of ϕ_r and ϕ_θ, t_i and k_i are calculated using Eqs. [21] and [22]. The calculated values of k_i and t_i are used to obtain w_h and Θ_h. Using the calculated pile head displacement and rotation, γ_1-γ_6 are calculated using Eqs. [13]-[15] and [17]-[19]. The calculated values of γ_1-γ_6 are compared with the assumed initial values and if the differences are more than the tolerable limit of 0.001, the same set of calculations are repeated with the calculated values of γ_1-γ_6 as the initial guesses. Iterations are continued until the values of γ_1-γ_6 between successive iterations fall below 0.001. A flowchart of the solution algorithm is given in Figure 4.

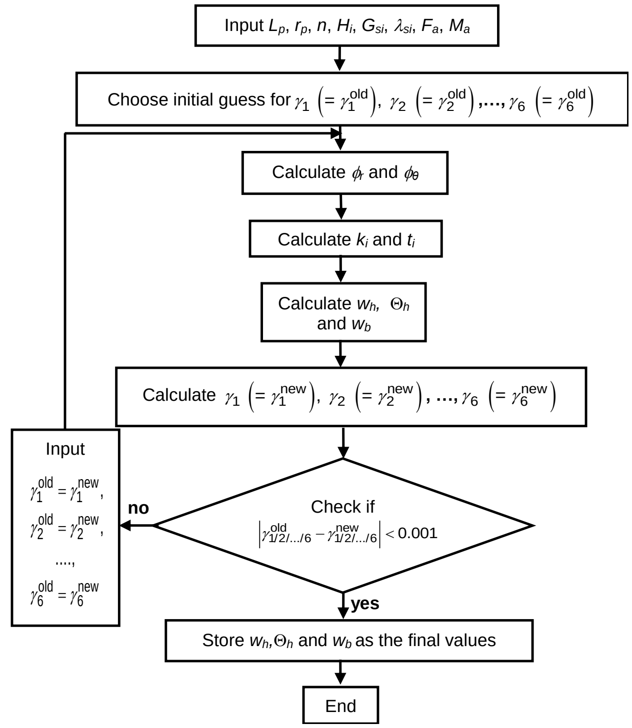

Figure 4. Solution flowchart

2.10 Modification of soil moduli

Randolph (1981) found that soil Poisson's ratio ν_s has a minimal effect on lateral pile response and therefore the pile response can be investigated by using an equivalent shear modulus which includes the effect of both soil elastic constants:

$$G_s^* = G_s(1 + 0.75\nu_s) \qquad [31]$$

However, it is observed that using the assumed soil displacement field given in Eqs. [5]- [7] the pile response is excessively stiff for soil Poisson's ratio close to 0.5. To avoid this excessive stiffness, Guo and Lee (2001) recommended setting ν_s = 0 irrespective of its actual value (which is the same as setting λ_s = 0) and indirectly take into account the effect of ν_s through Eq. [31].

3 RESULTS

The accuracy of the proposed analysis method is verified by comparing the pile response obtained from this analysis with that obtained from equivalent 3D FE analysis performed using the software ABAQUS (2010).

Figure 5 shows the normalized pile displacement profile for a large diameter rigid pile embedded in a three-layer soil profile — the details of pile and soil properties and the applied loading are shown within Figure 5. A difference of 8.96% occurred in the pile head displacement between the results obtained from the present analysis and FE analysis.

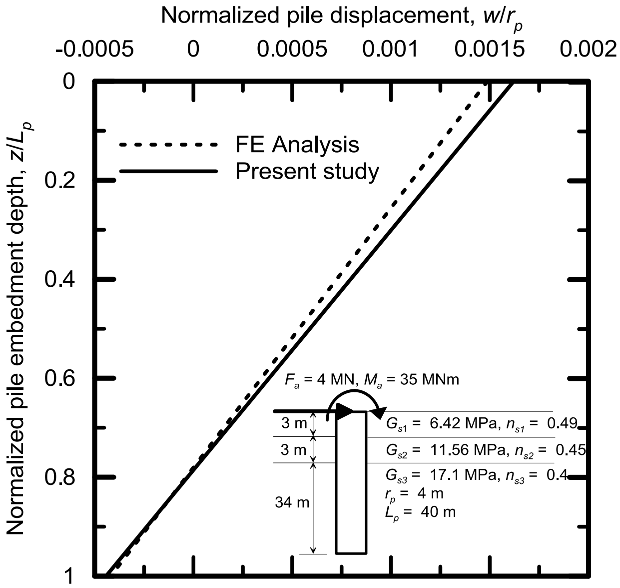

Figure 5. Comparison of normalized pile displacement as obtained from present analysis and FE analysis for a rigid pile in three-layer soil subjected to a lateral force and moment at the head

Figure 6 shows the normalized radial displacement u_r/r_p in soil at the ground surface (i.e., for z = 0) as a function of normalized radial distance in the direction of the applied load (i.e., for θ = 0) for the pile shown within Figure 5. Both the results obtained from the present analysis and FE analysis are plotted. As evident, the match between the results obtained from the present analysis and FE analysis are quite well.

4 CONCLUSIONS

A new continuum-based analysis of rigid circular monopiles for wind turbines embedded in multilayered elastic soil and subjected to a horizontal force and a moment at the pile head is presented. The equilibrium equation for the pile displacement and soil displacements are obtained using the principle of virtual work. Comparisons between the results obtained using the developed analysis and those from equivalent FE analysis show that the proposed new method works rather well. The new method requires much less computational effort when compared with the computational efforts required in FE analyses.

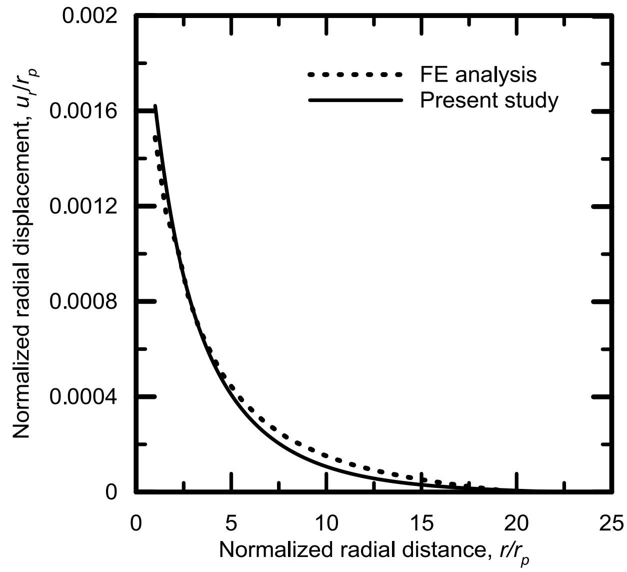

Figure 6. Comparison of normalized radial soil displacement at the surface obtained from present analysis and FE analysis for a rigid pile in three-layer soil subjected to a lateral force and moment at the head

REFERENCES

ABAQUS 2010. User's manual, version 6.10 simulia; *Dassault Systemes Simulia Corp., Providence, RI*.

Broms, B.B. 1964a. Lateral resistance of piles in cohesive soils. *J. Soil Mech. and Found. Div*., 90(2), 27–63.

Broms, B.B. 1964b. Lateral resistance of piles in cohesionless soils. *J. Soil Mech. and Found. Div*., 90(3), 123–159.

Guo, W. D., and Lee, F. H. (2001). "Load transfer approach for laterally loaded piles." *Int. J. Numer. Anal. Methods Geomech.*, 25(11), 1101–1129.

Higgins, W., Vasquez, C., Basu, D., and Griffiths, D.V. (2013). "Elastic solutions of laterally loaded piles." *J. Geotech. Geoenviron. Eng.*, 139(7), 1096-1103.

Haiderali, A., Cilingar, U., and Madabhushi, G. 2013. Lateral and axial capacity of monopiles for offshore wind turbines. *Ind. Geotech J.*, 43(3), 181-194.

Klinkvort, R.T., Springman, S.M., and Hededal, O. 2012. Scaling issues in centrifuge modelling of monopiles. *Int. J. of Phy. Modelling in Geotechnics*, 13(2), 38-49.

Klinkvort, R.T., Hededal, O. 2014. Effect of load eccentricity and stress level on monopile support for offshore wind turbines. *Can. Geotech. J.*, 51, 966-974.

Meyerhof, G.G., and Ranjan, G. 1972. The bearing capacity of rigid piles under inclined loads in sand. **1:** Vertical piles. *Can. Geotech. J*., 9, 430-446.

Motta, E. 2013. Lateral deflection of horizontally loaded rigid piles in elastoplastic medium. *J. Geotech. Geoenviron. Eng.*, 139 (3), 501-506.

Randolph, M.F. (1981). "The response of flexible piles to lateral loading." *Geotechnique*, 31(2), 247-259.

Zhang, L., Silva F., and Grismala, R. 2005. Ultimate lateral resistance to piles in cohesionless soil. *J. Geotech. Geoenviron. Eng.* 131(1), 78-83.